Indian Journal of Science and Technology, *Vol 9(15), DOI: 10.17485/ijst/2016/v9i15/72442, April 2016*

ISSN (Print) : 0974-6846
ISSN (Online) : 0974-5645

Computational Simulation of Blood Flow in Normal and Diseased Artery: A Review

R. Vinoth[1]*, Raviraj Adhikari[2] and D. Kumar[3]

[1]Department of Electronics and Communication Engineering, Manipal Institute of Technology, Manipal University, Madhav Nagar, Near Tiger circle, Manipal, Udupi - 576104, Karnataka, India.
vinoth.nair@manipal.edu

[2]Department of Mechanical and Manufacturing Engineering, Manipal Institute of Technology, Manipal University, Madhav Nagar, Near Tiger circle, Manipal, Udupi - 576104, Karnataka, India

[3]Department of Electronics and Communication Engineering, Periyar Maniammai University, Periyar Nagar, Vallam, Thanjavur - 613403, Tamil Nadu, India

Abstract

Background: Recent developments in Computational Fluid Dynamics (CFD) could help in the study of hemodynamics in the cardiovascular system that provides insight of variation of flow patterns with respect to changes in geometries. This paper focuses on the review of state of the art in the applications of computational fluid dynamics in the coronary artery. **Methods**: This article would give an overview about the computational fluid dynamics simulation of the blood flow in normal coronary artery, stenosed coronary artery, Coronary Artery Bypass Graft (CABG) and coronary stent. **Conclusion/ Application**: The computational fluid dynamics study would help the surgeon to get an idea about the severity of stenosed coronary artery, appropriate geometry and location of coronary artery bypass graft and coronary stent.

Keywords: Blood Flow, Computational Simulation, Coronary Stent, Diseased Artery, Hemodynamics, Normal Artery

1. Introduction

The heart is the key organ in the cardiovascular system. The blood flow in the cardiovascular system depends on the pumping action of the heart. This action makes the blood to flow in pulsatile nature. The aorta is the main blood vessel which supplies blood to the whole body, it branches off into two main coronary arteries called Right Coronary Artery (RCA) and Left Coronary Artery (LCA). These coronary arteries are divided into smaller arteries, which supply pure blood to the entire heart muscle'[1]. The RCA supplies oxygen - rich blood to the right side of the heart. The LCA supplies oxygen - rich blood to the left side of the heart, which branches into the Left Anterior Descending artery (LAD) and the Left Circumflex Artery (LCX).

Atherosclerosis is an inveterate inflammatory disease of the artery wall. This disease involves the formation of Plaques due to fatty deposition, cholesterol accumulation and calcium accumulation in arterial walls. This plaque formation narrows the arterial passage, restricting flow of blood[2] and increasing the risk of blockage of blood flow as shown in Figure 1a[3]. Coronary heart disease caused by atherosclerosis is the major cause of mortality from cardiovascular disease in much of the world's population, which is the leading cause of death in the United States[4]. Atherosclerosis in coronary artery could be treated by medical procedure or surgery. Dr. Andreas Gruentzig had introduced the angioplasty procedure and it is widely used today. In this procedure, the area of arterial occlusion due to plaque is distended by a surgical catheter that has a small balloon at its tip as shown in Figure 1bthen the plaque is mashed along the artery wall as shown in Figure 1c[3]. Stenting procedure was introduced by Dr. Julio Palmaz to treat atherosclerosis. Coronary stents physically open the canal of narrowed arterial segments as shown in Figure 2a[3]. In stenting procedure, a surgical catheter presents a balloon and also a surrounding stent to the location of the occluded area as shown in Figure 2b[3]. The balloon

*Author for correspondence

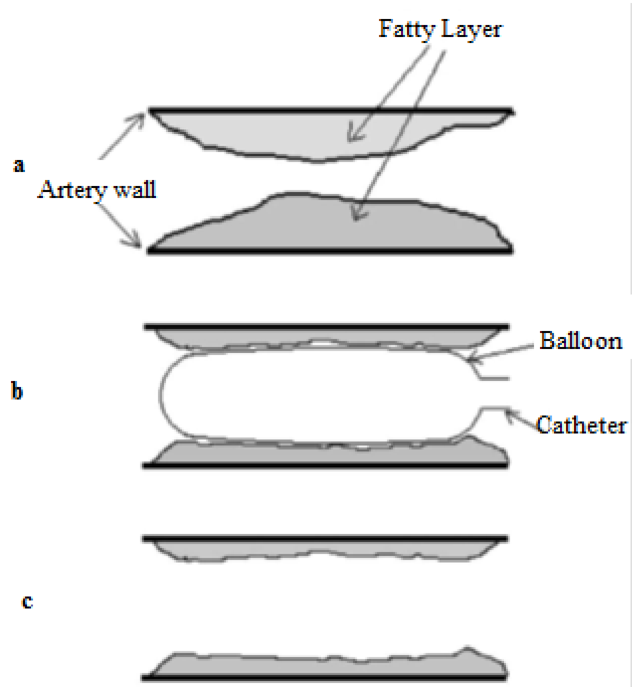

Figure 1. Angioplasty procedure. (**a**) fatty layer accumulates at and near the artery wall, (**b**) balloon inserted into the artery for expansion and (**c**) fatty layer pushed against the wall after balloon deflation and removal (Reprinted with permission from Elsevier).

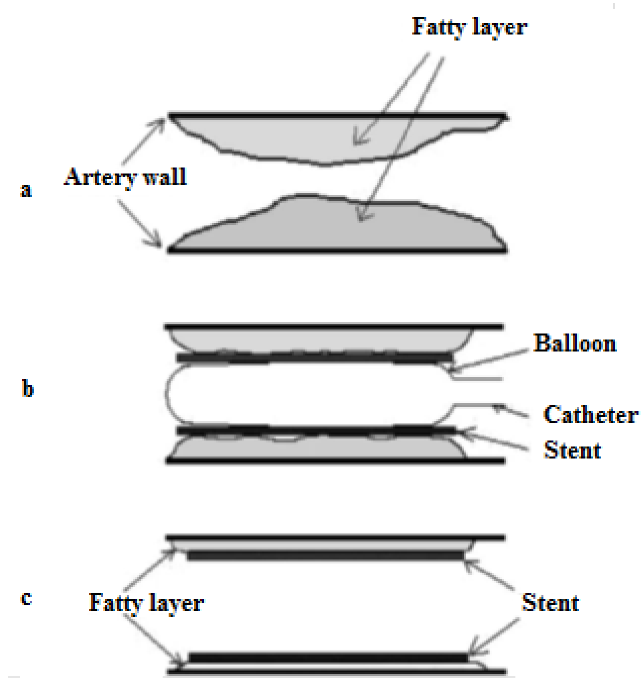

Figure 2. Stent deployment procedure. **(a)** fatty layer accumulates at and near the artery wall, **(b)** balloon surrounded by stent inserted into the artery for expansion and **(c)** fatty layer pushed against the wall and stent embedded into the wall after deflation and removal of the balloon (Reprinted with permission from Elsevier).

positions the stent, remains inflated for few seconds and then is deflated. Then, the expanded stent is implanted into the wall of the diseased artery and keeps it open as shown in Figure 2c[3]. High restenosis rate is the major drawback of angioplasty procedure. Restenosis is the formation of new occlusion at the site of the angioplasty and it affects the patients who have undergone balloon angioplasty procedure within few months. The restenosis rate is reduced to 20–30% by coronary stent procedure as compared to angioplasty procedure[5-7]. Drug-Eluting Stents have reduced the frequency of occurrence of restenosis[8]. Coronary artery bypass graft is a surgical procedure performed to restore the blood flow to deliver oxygen and nutrients to the heart muscle. In CABG (Coronary Artery Bypass Graft), the cardiac surgeon creates new route around stenosed artery by bridging it with a replacement vessel. Intimal hyperplasia due to poor hemodynamics could affect the bypass graft[9-12]. Atherosclerosis condition is changed by hemodynamics of blood, such as shear stress, oscillatory shear index (OSI), wall shear stress (WSS) and WSS spatial gradient (WSSG)[13-22]. These hemodynamics parameters are powerfully influenced by flow conditions, which are mostly dependent on the geometry of artery[23,24]. These parameters are used to afford a better judgment of the severity of coronary stenosis disease[25-27]. The CFD model could be used to depict the blood flow patterns in different anatomical geometries[28-36]. In the forefront of research of biological fluid flows, CFD simulation of hemodynamics is very important[37].

The imaging methods used in clinical applications can provide onlythe anatomic significance of Coronary artery disease (CAD). The flow rate and pressure data information of CAD can be determined by angiography and MRI method, but other parameters cannot be determined. The rich hemodynamic information of coronary heart disease can be determined by CFD analysis. Hence, the application of CFD techniques to the study of hemodynamic parameters of coronary heart disease has grown tremendously in the recent years.

In this review, perspective on computational fluid dynamics simulation of the blood flow in normal coronary artery, stenosed coronary artery, Coronary Artery Bypass Graft (CABG) and coronary stent are discussed.

2. Methodology

The developed imaging techniques are used to describe the three-dimensional (3D) vessel morphology. The imaging and CFD techniques are coupled together to create the CFD models of the pathologic vessels[38]. Figure 3 shows the method of CFD model generation of coronary artery.

A CFD model generation includes the preprocessing, solving the governing equations numerically, and post-processing to present the results. Generally the 3D Geometry of coronary artery can be created by two methods. In the first method, the coronary artery contours will be extracted by image processing technique from tomographic images such as magnetic resonance imaging (MRI), magnetic resonance angiography (MRA), computed tomography (CT) images and ultrasound (US)[39-44]. Then, the extracted contour points of coronary artery will be imported into a CAD (Computer - Aided Design) program to create the 3D geometry. In the second method, the dimensions of patient's coronary artery will be obtained from any imaging techniques such as MRI, MRA and CT. The 3D geometry of the coronary artery will be created by CAD software package from the obtained dimensions. Then, these CAD models will be meshed and CFD analysis will be carried out with appropriate boundary conditions and blood flow parameters. Even the 3D geometry of coronary artery reconstructed from imaging techniques to represent the domain of interest, proper boundary conditions are necessary for CFD simulations. Even though some instruments are used to measure inflow velocity, outflow velocity, flow and pressure waveforms of coronary artery, obtaining realistic boundary condition is probably the biggest challenge in CFD simulation of coronary blood flow. In this regard, the boundary conditions obtained from the literature, *in vitro* and *in vivo* measurements have been prescribed for CFD simulation. The CFD technique numerically solves continuity equation (1) and Navier-Stokes equation (2) to measure hemodynamic parameters of blood flow in the coronary artery models.

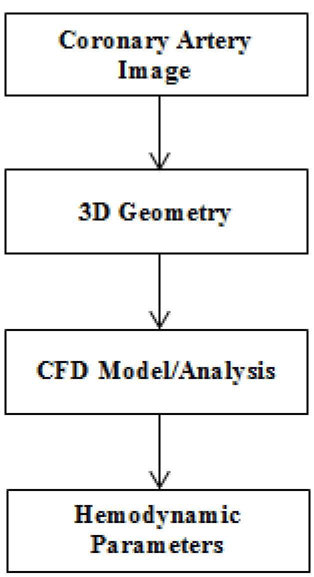

Figure 3. Flow diagram of the CFD model generation.

$$\frac{\partial \rho}{\partial t} + \frac{\partial}{\partial x_j}\left(\rho u_j\right) = 0 \tag{1}$$

$$\frac{\partial}{\partial t}(\rho u_i) + \frac{\partial}{\partial x_j}\left(\rho u_i u_j\right) = \frac{\partial}{\partial x_j}\left[-p\delta_{ij} + \left(\frac{\partial u_i}{\partial x_j} + \frac{\partial u_j}{\partial x_i}\right)\right] \tag{2}$$

where u is the blood velocity in the lumen region, ρ is the density of blood, p is the blood pressure and μ is the viscosity of the blood flow.

3. Clinical Application of CFD in Coronary Artery

3.1 CFD in Normal and Stenosed Coronary Artery

Wei Yin et al[45]. developed a CFD model of the left coronary artery under normal and disease conditions. They have calculated blood flow velocity, blood flow induced shear stress from the developed model and then used the calculated shear stress to stimulate vascular endothelial cells in vitro. The CFD models of the left coronary artery under normal, 30%, 60% and 80% stenosis conditions were built. The different Stenosis conditions were modeled in the left anterior descending artery and it occurred at 8 mm downstream of the bifurcation. The CFD analysis of the flow field was carried out for the developed models with blood as non-Newtonian viscoelastic fluid and the inlet velocity waveform with the flow velocity ranging between 0.2 and 30 cm/sec with a period of 0.84 sec. The study revealed that, the flow in constricted vessels sped up at the stenosis throat, recirculation zones built up behind the stenosis, and recirculation zones grow bigger as stenosis condition increases. The wall shear stress in the stenosed condition was much higher than that under normal conditions as shown in Figure 4.

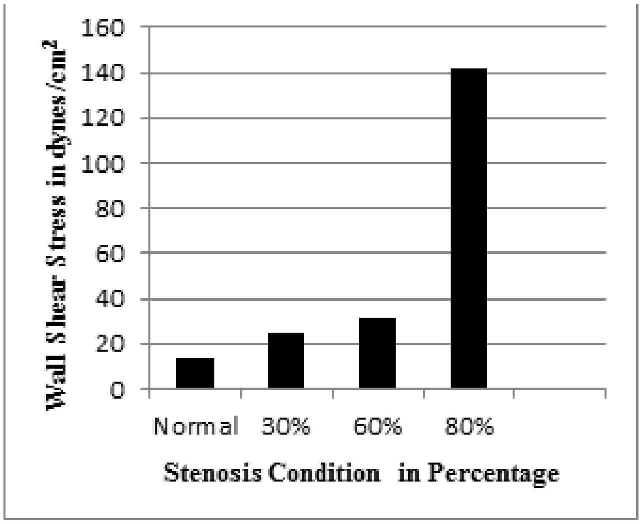

Figure 4. Wall shear stress distribution.

Yunlong Huo et al[24]. studied the effect of vessel wall compliance on the hemodynamic parameters of pulsatile blood flow pattern. They developed 3-D finite element model of Right Coronary Artery (RCA) tree from computed tomography imaging data and measured the wall motion due to vessel compliance. The continuity and Navier-Stokes equations were solved to calculate velocity and pressure field of blood flow. The hemodynamic parameters such as WSS, WSSG and OSI were examined. The authors reported that OSI was small in the epicardial RCA tree. The time - averaged WSS and WSSG in the main trunk of RCA tree were affected by motion due to vessel compliance in little amount. This WSSG was decreased by motion due to vessel compliance at bifurcations.

Abraham et al[46]. quantified the effectiveness of debulking in small arteries. The geometries of the plaque narrowed and plaque freed arteries were built from the ultrasonic images. Fluid analysis was carried out for these models. The authors detected that, the blood flow rate was increased in the plaque freed artery as shown in Table 1. The shear stress on the artery wall was higher in the plaque freed artery than the plaque narrowed artery.

Frank et al[47]. generated CFD model of the Left Anterior Descending (LAD) coronary artery with bifurcation and second diagonal. The relationship between shear stress (SS), wall thickness (WT) and remodeling was studied in the computational model. They detected that the effect of the side branch on the SS distribution in the main branch reduced reasonably. The authors determined that there was expansive remodelling and plaque in the low SS region of the proximal region of the model, but they observed lumen narrowing in the distal portion.

Table 1. Mass flow rates for pre-debulked and debulked artery (Reprinted with permission from Elsevier).

Flow(grams/cycle)	Pre-debulked	Debulked	Ratio:Post/ Pre
Systole	0.0353	0.0859	2.43
Diastole	0.0186	0.0521	2.80
Net	0.0166	0.0338	2.04

Brunette et al[48]. estimated the shear stress distribution and secondary flows in the mildly stenosed coronary artery. The 3D stenosed coronary artery phantom was developed from a whole volume Particle Image Velocimetry (PIV) method. The 3D whole volume velocity data was obtained from the 2D velocity stacked data. The shear stress distribution and secondary flow were calculated from the derived 3D velocity data. The authors found, the shear stress exceeds the normal value and atheroprotective range and secondary flows were started at an early stage of stenosed pathology.

Ryo Torii et al[49]. studied the effect of catheter on blood flow in a coronary artery for different catheter probe diameters and flow status. The model of the coronary artery developed with curved pipe of 3.0 mm diameter and the model of the catheters developed as curved cylinders for the diameters of 0.30, 0.60 and 1.0mm. At both the ends of the curved pipe, a straight pipe with 30mm of length was joined to provide the correct flow conditions. The authors assumed that probe tip was fixed half - way along the curved section and the catheter remained at the center of the coronary artery. They solved CFD equations for the developed model considering blood flow as Newtonian, incompressible and laminar. The authors found the pressure values were increased by the insertion of catheter probe based on its diameters as shown in Figure 5 and velocity-pressure phase lag were decreased.

Perktold et al[50]. developed computational model of the left anterior descending coronary artery with its first diagonal branch (DI). Then the authors created experimental model of the replica of the computational model using silicone rubber. They simulated pulsatile flow field in computational model and measured flow parameters in experimental model using laser Doppler anemometry. The authors compared velocity profile and WSS profile

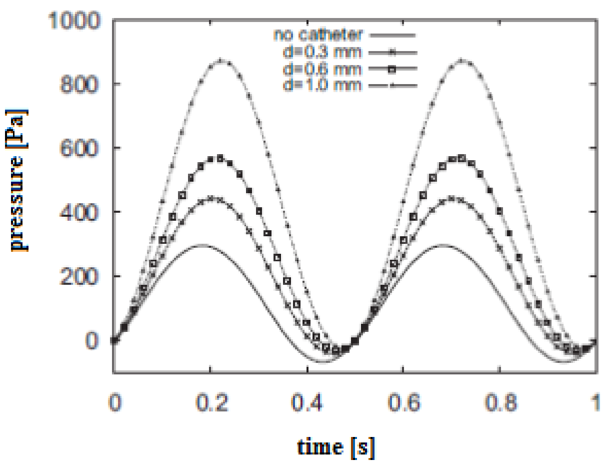

Figure 5. Pressure profile (Reprinted with permission from Elsevier).

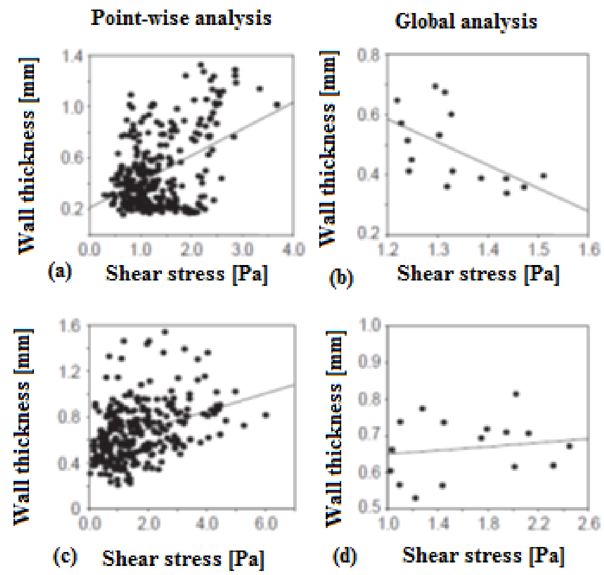

Figure 6. Relationship between wall thickness and shear stress of two segments. point-wise analysis (a, c), global analysis (b, d) (Reprinted with permission from Elsevier).

for both models. They found that the axial velocity results from computational analysis were comparable with the measured values during experiments.

Simone Melchionna et al[51]. simulated the blood flow in the human coronary artery system using MUPHY simulation package and computed the endothelial shear stress (ESS). The authors reported the great structure of ESS in the nearby region of main coronary bifurcation.

Sasa Kenjeres[52] analyzed the impact of strong non-uniform magnetic field on the blood flow patterns in realistic artery. The author developed numerical model of human right-coronary artery with different stenosis rate and simulated pulsatile blood flow with and without magnetic field. From the simulated results it was concluded that the substantial magnitude of applied magnetic field had changed the local pressure values and significant secondary flow patterns were obtained due to imposed non-uniform magnetic field.

Wentzel et al[53]. compared the results of point-wise and global analyses of the raw data to understand the effect of shear stress (SS) in initiation of atherosclerosis. They generated CFD model of human coronary artery by assuming blood as non-Newtonian fluid. Shear stress and Wall thickness (WT) were measured for sixteen different circumferential locations. The authors studied 24 segments from 12 coronary arteries. From the comparison the authors concluded that there was a positive relation between WT and SS for 21 segments in point-wise analysis but the global analysis produced 38% inverse relation between them as shown in Figure 6.

Ernst Wellnhofer et al[54]. studied the effect of circular and elliptical cross-section methods of coronary artery lumen reconstruction. They reconstructed three right coronary arteries with different resolutions. Out of three coronary arteries one artery was normal, one artery with a block and another with dilated coronary atherosclerosis. The CFD models of these coronary arteries were developed by a control volume finite element method. The authors reported from the CFD simulation, that the WSS distributions were identical for both high and low resolution reconstruction methods, the range of pressure loss difference was from 2.5% to 8.5% for the two methods and the mean WSS was 4.6 Pa, 8.8 Pa and 1.3 Pa for normal, blocked and dilated cases respectively.

Soulis et al[55]. investigated the main blood flow parameters such as wall pressure (WP), WSS, wall pressure gradient (WPG), WSSG and molecular viscosity of the human Left Coronary Artery (LCA) tree model. They developed CFD model of LCA tree which includes the left main coronary artery, the Left Anterior Descending (LAD) artery branch, the Left Circumflex Artery (LCX) branch and their major branches. From the simulation they got low WP, WPG, WSS, WSSG and high molecular viscosity values at bifurcations and between proximal and distal LCA tree area. The authors concluded that the variations in blood flow parameters were the major components in generation and progression of atherosclerosis.

Thanapong Chaichana et al[56]. examined the influence of angulations of LCA on hemodynamic parameters. They developed twelve models of LCA with different angulations. Out of twelve models four models were realistic models and eight models were simulated one. These models include left main artery, LAD and LCX artery branches. The CFD simulation was carried out for 1.0 s of pulsatile flow in all the models and WP, WSS, WSSG and velocity flow pattern were obtained. They observed the reduced wall pressure values when blood flows from the left main artery to the bifurcating area and affected flow patterns for the wider angle models. For wide angles of bifurcation they got a low WSSG values at left bifurcations and concluded that there was a better positive correlation between blood flow dynamic changes and coronary angulations.

Beier et al[57]. developed CFD model of left main coronary artery bifurcation to compare flow measurements with 4Dphase contrast (PC) magnetic resonance imaging flow measurements. The authors declared that the phase contrast (PC) magnetic resonance flow measurements show good quantitative and structural similarity to CFD flow measurements. They obtained the standard deviation of the differences between the PC and CFD flow data was less than 10% and concluded that CFD may be useful tool for the identification of regions of artifact in phase contrast magnetic resonance flow data.

3.2 CFD in Coronary Artery Bypass Graft

Leok Poh Chua et al[58]. investigated the blood flow characteristics of complete anastomosis model. They developed a 3D model of complete anastomosis with both the proximal and the distal parts which could be used in CABG operation. Then, they computed three dimensional laminar flow characteristics by assuming blood as Newtonian, homogeneous and incompressible fluid. The authors found out, the velocity gradients and wall shear stress gradients were high in the distal anastomosis part of the graftas shown in Figure 7 and Figure 8 respectively and flow has more changes at distal part than the proximal part.

They concluded that high wall shear stress gradient region at the bed of coronary artery and the toe could be reduced with smaller grafting angle and smooth geometry.

Leok Poh Chua et al[59]. studied the flow characteristics in cuff-like sleeve models. Sleeve models are the mechanical connectors between the bypass graft and host artery at the distal anastomosis. They designed three models

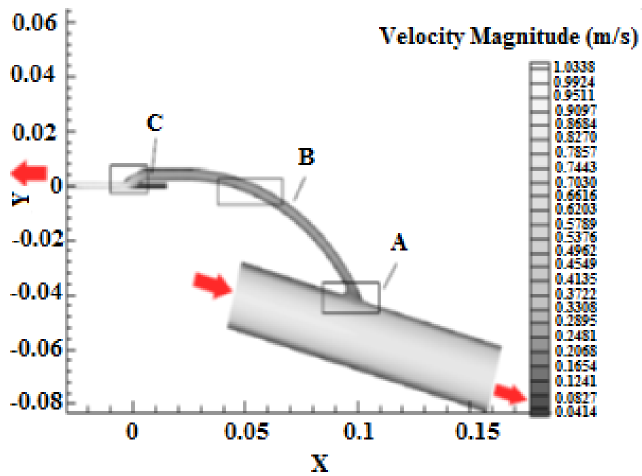

Figure 7. Velocity contour within the symmetry plane (Reprinted with permission from Elsevier).

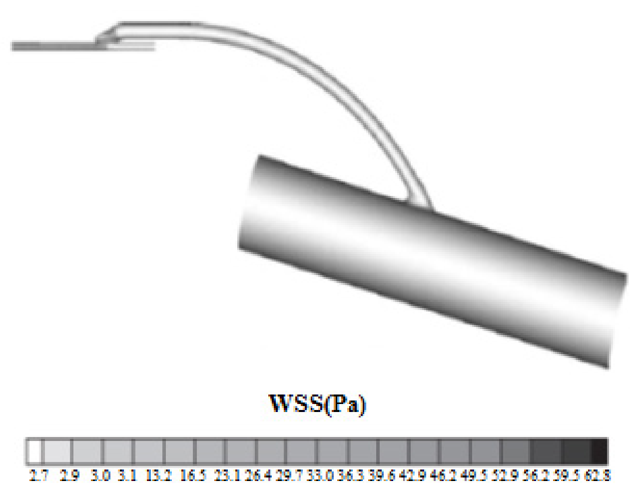

Figure 8. Wall shear stress distribution of anastomosis model (Reprinted with permission from Elsevier).

which included graft, sleeve, proximal host artery and distal host artery. The first model was the baseline model, the height of the sleeve increased in the second model and the diameter of the sleeve increased in the third model. The computations were made in the designed models by assuming as Newtonian and incompressible fluid with laminar flow characteristics. The authors found that, the volume of the first model was larger than the conventional bypass models, the volume of the second model was larger than first model and third model would result in slower fluid flow.

The coronary artery anastomotic models with different diameter ratio and angle between the graft and host artery were investigated numerically by Xiong and

Chong[60]. The authors have designed six coronary anastomotic models by varying diameter with constant angle and by varying angle with constant diameter. The flow patterns, WSS, OSI, spatial and temporal WSS gradients (SWSSG and TWSSG) were compared for all six models. From these comparisons the authors concluded that the diameter ratio was the important geometric parameter in coronary revascularization surgeries and the effect of the diameter ratio was larger than that of angle in hemodynamic analysis.

Shim and Kamm[61] described the blood flow pattern through the coronary bypass shunt. The bypass shunt directly connects the left ventricular to the distal portion of the occluded coronary artery. They mainly concentrated on the effect of shunt angle on the blood flow patterns. The authors solved three dimensional computational equations for blood flow through a bypass shunt with three different angles (45º, 67º, 90º) between shunt and artery. The results revealed a recirculating region near the junction between the coronary artery and shunt, largest secondary flow with 90º shunt angle than other shunt angle and maximum pressure drop between inlet to outlet was directly proportional to shunt angle.

Bertolotti and Deplano[62] analysed the blood flow patterns in anastomosis model of a stenosed coronary artery bypass graft. They developed model of normal coronary artery and artery with stenosis for three different distances upstream from the heel. Three flow rates have been used for the four models of coronary artery. From simulation the authors found the resultant residual blood flow from the constricted artery was similar to flow of confined jet shape and Kakos et al[63]. stated that it reduced progressively. At the distal region from the stenosis, the velocity profiles became bell and conical shape. The recirculation zone was observed at the walls of the artery and the peak velocity was skewed at downstream from the toe.

Politis et al[64]. studied the relation between the grafts and coronary artery flows with respect to spatial and temporal deviation of velocity and WSS distribution. They developed geometrical model of composite arterial coronary graft (CACG) with T and Π – graft configurationas shown in Figure 9. These models were generated with 25%, 50%, 75% of stenosis conditions and also normal condition. The authors introduced different grafting distances and inflow rate ratios in their model. The finite volume method was applied to solve the flow equations. The velocity contours were compared for the T-configuration graft

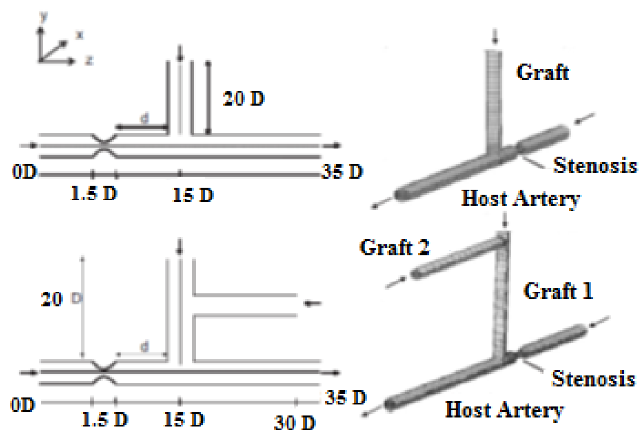

Figure 9. Geometrical models and computational meshes of CACG (Reprinted with permission from Elsevier).

with 75% stenosis and normal case. The flow produced non-uniform

velocity distribution after the bifurcation in without stenosis case. In the case of stenosis the velocity value was low at the walls after the stenosis. In the Π – graft configuration, the magnitude of velocity varied but overall velocity distribution appeared same. The velocity field had nearly parabolic in shape for 25% stenosis and conical in shape for 50% stenosis conditions. The recirculation zone and low velocity values were obtained at the toe portion of the 75% stenosis model. For different flow rate ratios the similar output were obtained for the velocity variation from the center of host artery[62,65,66]. The WSS distributions were calculated for four different points in T-graft configuration and five points in Π – graft configuration as shown in Figure 10. During systole the WSS increased suddenly at the points on the lower wall of the native artery but at the points on the upper wall the WSS was reduced. The WSS variation was uniform after the stenosis during diastole. The similar results were obtained by Bertolotti et al[67].

Lei et al[20]. and Freshwater et al[68]. reported that the rheology of human blood, graft surface properties, the ratio between artery and graft diameters, the structure of the artery and graft junction were the important parameters for the initiation and progression of restenosis.

Kim et al[69]. developed the CFD model of an anastomosis end-to-end configuration and simulated the blood flow through the model by assuming blood as Newtonian fluid, steady flow conditions and wall as rigid. The authors observed the flow separation region at 2mm distal to the

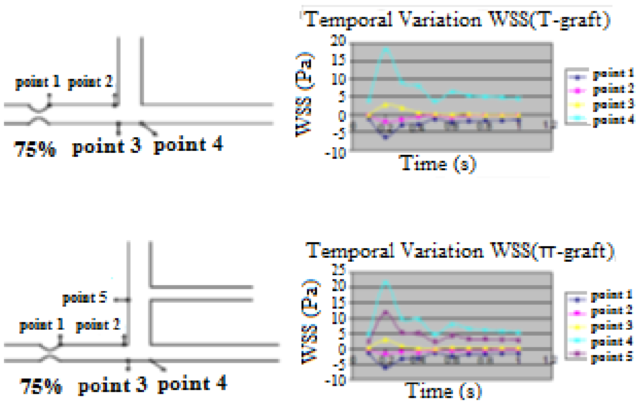

Figure 10. Spatial shear stress distribution in T and Π – graft configurations for 75% stenosis case (Reprinted with permission from Elsevier).

artery junction when the pressure difference between inside and outside of the artery was high.

Kute and Vorp[70] examined the result of proximal artery conditions on the blood flow dynamics at the distal end-to-side anastomosis. They solved the flow equations by the finite volume method and calculated WSS and WSSG. The authors concluded that the proximal artery flow condition was a crucial determinant of the hemodynamics at the distal anastomosis of end-to-side configuration bypass grafts.

Bonert et al[71,72]. numerically simulated the fluid flow of side-to-side coronary artery bypass graft and calculated shear stress distribution. They computed the difference in hemodynamics of end-to-side and side-to-side configurations. The authors reported that the hemodynamics of end-to-side was better than the side-to-side anastomosis and hemodynamics of parallel form of side-to-side anastomosis was better than the non-parallel form.

The influence of graft and host diameter ratios on WSS and the blood flow parameters in CABG was investigated by Qiao and Liu[73]. The authors developed three different models with graft diameter equal to, larger than and smaller than the coronary artery diameter. They simulated pulsatile blood flow in those three models and concluded from the simulation the large diameter model can produce good hemodynamics with large positive longitudinal velocity, large WSS and small WSSG. The authors reported that isodiametric or larger diameter graft was good, but there was no major difference in temporal parameters of WSS between all the three models. They suggested that the better anastomosis configurations are required to improve the patency rates of CABG.

The many researchers had undertaken CFD simulation with different boundary conditions to analyze the influence of CABG configurations and various flow conditions on hemodynamics parameters. The boundary conditions assumed by a few authors as shown in Table 2[74].

Table 2. Different boundary conditions of CFD simulation with common assumption artery wall as rigid wall and No-slip condition (Reprintedwith permission from Elsevier).

Authors	Steady state	Transient state	Constant outlet pressure	Newtonian Fluid	Non-Newtonian Fluid , power law, carreau, walburn-schenck, casson, Generalized power law model
Bertolotti and Deplano [61]	✓		✓	✓	
Chen et al. [86]	✓		✓	✓	✓
Do et al. [87]		✓	✓	✓	
Freshwater et al. [68]		✓	✓	✓	
Lee et al. [88]	✓		✓	✓	
Politis et al. [89]	✓		✓	✓	
Politis et al. [64]		✓	✓	✓	
Sankaranarayanan et al. [36]		✓	✓	✓	
Vimmr and Jonasova [90]	✓		✓	✓	✓
Zhang et al. [91]			✓		

3.3 CFD in Stented Coronary Artery

Benard et al[75]. investigated the three dimensional flow of a stented coronary artery with the assumptions, rigid wall and steady inlet flow. They had considered the blood as a non-Newtonian fluid. They presented the velocities, WSS and WSSG from the simulations. The authors concluded that, the stent structure had no influence on velocities located on the centre of artery, low WSS close to stent branches and maximum WSSG near stent wire.

Garcia et al[76]. studied the effect of blood flow dynamics parameters on the development of coronary restenosis. The authors numerically simulated the blood flow dynamics of a group of seven patients with a stent in the RCA just after stent implantation and six months later. The authors reported, in six out of seven patients the wall thickness had increased whereas the wall shear stress was lowas shown in Figure 11 and Figure 12. The normal wall regions were not affected by the coronary stent and from intra–stent and extra-stent regions the restenosis occurred where the wall shear stress was low.

Hao-Ming Hsiao et al[77]. reported the influence of rheological properties and pulsatile flow on hemodynamic parameters of the intra-stent blood flow. They have simulated axisymmetric and 3-D stented artery CFD models with the assumptions Newtonian, non- Newtonian, pulsatile and Steady-state flow. The velocity waveform of the RCA was taken from data reported in the literature by Bertolotti et al[67]. for their pulsatile and Steady-state flow

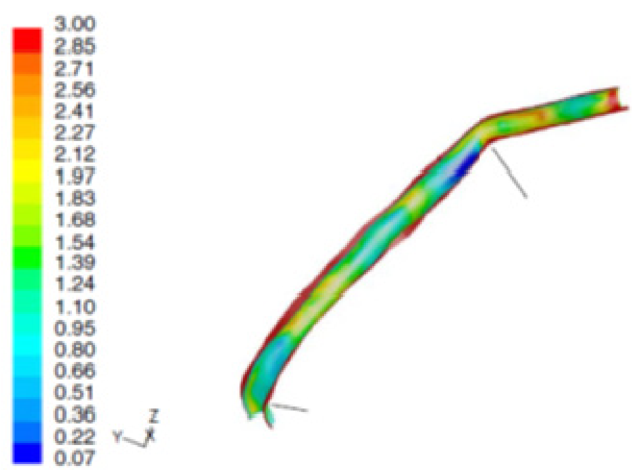

Figure 11. Contours of wall shear stress at the wall artery, immediately after stent implantation. The wall thickness is shown in violet colour (Reprinted with permission from Elsevier).

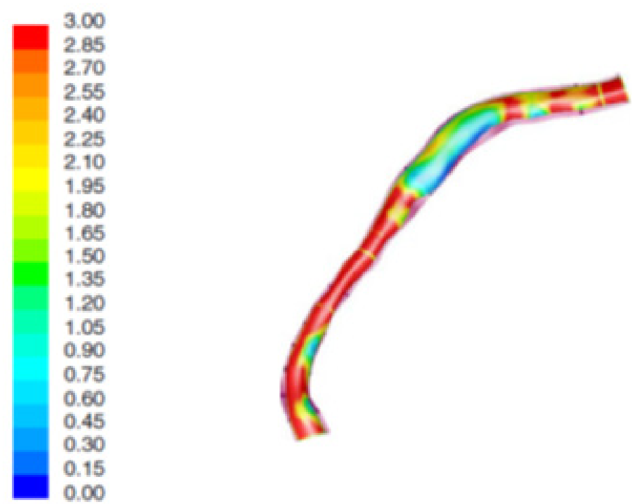

Figure 12. Contours of wall shear stress at the wall artery, after six months of stent implantation. The wall thickness is shown in violet colour (Reprinted with permission from Elsevier).

simulation. The authors proposed that the steady-state Newtonian flow simulation suited for intra-stent blood flow, which could reduce the computation time.

John et al[78]. studied sharp changes of WSS distributions in curved coronary arteries after stent implantation, which implanted stent either conform to or makes straightening of the artery. They have generated 3D coronary artery CFD models with stent based on measurements from canine left anterior descending coronary arteries. The authors concluded from the computational simulation, the implantation of the stent made straightening of the curved artery, which altered spatial distributions of WSS. Those WSS variations were noticeable in the proximal and distal portion of the stent.

Claudio Chiastra et al[79]. found the hybrid meshing method produced the accurate CFD results on the 3D complex geometries within the shortest computational time. They developed 3D model of stented coronary artery with bifurcation and this model was meshed with hybrid meshing technique to analyse the different hemodynamic parameters created by a final kissing balloon (FKB) procedure performed with the types of side branch access (proximal or distal). They performed transient CFD simulations to examine the WSS, velocity and helicity fields. The authors reported that the area exposed to low time-averaged wall shear stress (TAWSS) was 84.7% in the distal access case but in the proximal access case it was 88.0%. They concluded that from the WSS distribution on the artery wall, velocity and the helicity field results the distal access method was better than the proximal access method.

Vahab Dehlaghi et al[80]. analysed the influence of stent geometry on blood flow patterns in 2D and 3D CFD models of human coronary artery with stent. Shear stress and blood velocity profiles were calculated for stented artery, pre-stent and post-stent regions. The authors studied the effect of the ratio of stent strut spacing to the stunt strut height (W/H) where W was the stent inter-ring width and H was the stent wire thickness, the effect of the stent strut shape, effect of the curvature angle, effect of the number of rings on the circumference of the stent and Reynolds number, effect of the flow divider and effect of the real structure of the stent on blood flow parameters. The authors found that the stent strut spacing was responsive to WSS distribution between the struts. The WSS value changed according to the ratio W/H and the flow separation zone as shown in Figure 13. In this graph the authors have taken the ratio between shear stress values in stent strut space and in the artery without stent on the vertical axis and the ratio W/H on the horizontal axis. The circular, rectangular and triangular shape wire struts were compared by the authors to examine the influence of the shape of the strut on the near wall blood flow parameters. They got lowest WSS for rectangular shape strut and highest WSS for the circular shape strut. They concluded that WSS values were changed with respect to strut shape as shown in Figure 14. The authors also concluded that

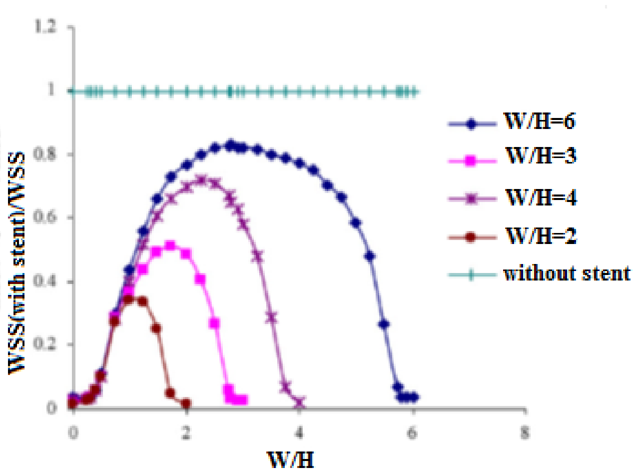

Figure 13. Influence of the ratio between W and H on the WSS value between stent struts (Reprinted with permission from Elsevier).

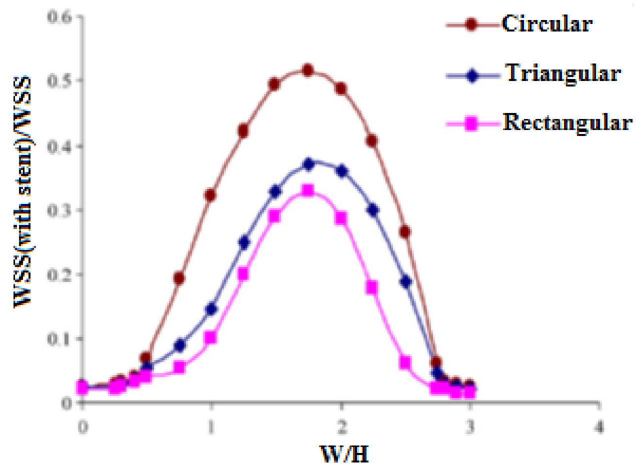

Figure 14. Influence of the stent strut shape on the WSS between stent struts with the ratio between W and H equal to 3 (Reprinted with permission from Elsevier).

the difference in WSS values of the inner and outer wall were increased with increase in arterial curvature angle in curved stented coronary artery models, beyond seven rings along the circumference of the stent the length of the flow separation zone did not depend on the number of stent rings, the length of separated flow zone was increased with increase in Reynolds number, the shear stress distribution within the flow divider were more than the shear stress in the stent without flow divider and also the flow divider increased the WSS in the stented coronary artery segment.

Hao-Ming Hsiao et al[81]. analysed the changes in WSS distribution by stent geometry and stent design pattern. The authors developed CFD models of coronary artery with five different commercial stents and simulated blood flow through the models. They concluded that the variations in strut width or crown radius could vary WSS marginally but strut thickness could vary WSS significantly, the stent design pattern alone could not make any changes in WSS distribution and the stent hemodynamic character could be improved by thinner stent design.

Murphy and Boyle[82] investigated the influence of increasing levels of physiological realism on the blood flow parameters in the CFD models of the coronary arteries with stents. They generated CFD model of LAD coronary artery with the Gianturco-Roubin II (GR-II) coil stent (Cook, USA) and with the Palmaz-Schatz (PS) slotted tube stent (Johnson & Johnson, USA). The CFD analysis carried out for the developed model of coronary artery with normal stent size, oversized stent and oversized stent including tissue prolapse between the stent wires. The authors measured WSS and WSSG presented on the arterial tissue for six test cases. The authors reported that the oversized model with both stents produced much better low WSS area than normal model but low WSS measured around the stent wires in the normal model. The oversized with prolapse model produced modest low WSS than oversized model for both stent types and this model gave the highest WSSG than other two models.

Rossella Balossino et al[83]. studied the effect of stent on the blood flow dynamics in coronary artery. They developed coronary artery model with different stent designs, different strut thickness and plaque. The CFD analysis was carried out with the pulsatile flow condition and WSS distribution was studied. The authors observed almost same oscillatory WSS in all stent models and maximum WSS on the stent surface. They found highest values of WSS spatial distribution at the centre of the artery wall and this value defined by stent strut.

Morris et al[84]. developed CFD model of coronary tree with disease to predict myocardial fractional flow reserve (FFR). They measured FFR of nineteen patients with stenosis and stent using rotational coronary angiography. The authors generated CFD model of pre- and post-stenting coronary artery from angiographic images and measured FFR from CFD analysis with generic boundary conditions. The measured fractional flow reserve (mFFR) and virtual fractional flow reserve (vFFR) values were compared. The authors found that on average, the vFFR values deviated from mFFR by 0.06 and both were closely correlated.

Feng Gaoet al[85]. studied fluid dynamics factors in coronary artery bifurcation models before and after stenting procedure. The pre- and post-stenting CFD models of coronary artery bifurcation were generated from CT imaging technique. The authors obtained higher WSS value and velocity value at the stenosis region without stent. They got fluid dynamic values in stented model similar to normal coronary artery.

4. Conclusion

The published literature on the application of CFD to the blood flow in normal and stenosed coronary artery, Coronary Artery Bypass Graft and coronary stent were reviewed. The measured parameters from the CFD study could help in understanding the severity of coronary stenosis and optimization of drug delivery, to suggest valid guideline on construction of proximal and distal coronary anastomosis before surgery. The parameters measured from the CFD modeling of the coronary artery with stent could help to determine the exact size, orientation and effectiveness of the stent, this prior information would reduce the vascular injury and surgery time. Hence the CFD is a valid and powerful simulating tool for understanding of cardiovascular flows and it could support the quantitative measurement of clinical parameters and also assist the surgeons for exact interventional or surgical planning.

A numerous investigations have been carried out on the CFD simulation of the blood flow in normal and stenosed coronary artery, Coronary Artery Bypass Graft (CABG) and coronary stent. To the best of authors knowledge, the study on the CFD analysis of the blood flow in multiple stenosis condition in the coronary artery had not been attempted and also very few studies have been conducted with realistic conditions such as constitutive material models, Non-Newtonian fluid. The CFD study of multiple stenosed coronary arteries would provide deep insight into the response of an actual coronary artery under different flow and boundary conditions. The simulation of realistic conditions in patient-specific arterial models could provide a useful scientific basis for the determination of status of the diseased artery more precisely and optimization of stent in the coronary artery stent treatment.

5. References

1. Ghassan S, Kassab. Design of coronary circulation: A minimum energy hypothesis. Computer Methods in Applied Mechanics and Engineering. 2007; 196(31):3033-42.
2. Shathesh S, Durairaj M. An Intelligent Hybrid Mechanism to Predict the Risk of Cardio Vascular Disease. Indian Journal of Science and Technology. 2016; 9(4):1-8. Doi: 10.17485/ijst/2016/v9i4/82278.
3. Gay M, Zhang L, Liu WK. Stent modeling using immersed finite element method. Computer Methods in Applied Mechanics and Engineering. 2006; 195(33-6):4358–70.
4. Minino AM, Heron MP, Smith BL. Deaths: preliminary data for 2004. National vital statistics reports. Hyattsville MD: National Center for Health Statistics. 2006; 54(19):1-49.
5. Fischman DL, Leon MB, Baim DS, Schatz RA, Savage MP, Penn I, Detre K, Veltri L, Ricci D, Nobuyoshi M, Cleman M, Heuser R, Almond D, Teirstein PS, Fish RD, Colombo A, Brinker J, Moses J, Shaknovich A, Hirshfeld J, Bailey S, Ellis S, Rake R, Goldberg S. A randomized comparison of

coronary-stent placement and balloon angioplasty in the treatment of coronary artery disease. The New England Journal of Medicine. 1994; 331(8):496-501.

6. Serruys PW, De Jaegere P, Kiemeneij F, Macaya C, Rutsch W, Heyndrickx G, Emanuelsson H, Marco J, Legrand V, Materne P, Belardi J, Sigwart U, Colombo A, Goy JJ, Van den Heuvel P, Delcan J, Morel MA. A comparison of balloon expandable-stent implantation with balloon angioplasty in patients with coronary artery disease. The New England Journal of Medicine. 1994; 331(8):489-95.
7. Gottsauner-Wolf M, Moliterno DJ, Lincoff AM, Topol EJ. Restenosis - an open file. Clinical Cardiology. 1996; 19(5):347–56.
8. Sandeep, Patted SV, Halkatti Prabhu, Modi Ranjan. Effect of Stent Length on Clinical Outcome in Patients with Coronary Artery Disease. Indian Journal of Science and Technology. 2015; 8(4):329-36.
9. Grondin CM, Lesperance J, Bourassa MG, Campeau L. Coronary artery grafting with the saphenous vein or internal mammary artery. Comparison of late results in two consecutive series of patients. Annals of Thoracic Surgery. 1975; 20(6):605–18.
10. LoGerfo FW, Soncrant T, Teel T, Dewey CF. Boundary layer separation in models of side-to-end arterial anastomoses. Archives of Surgery. 1979 Dec; 114(12):1369-73.
11. Crawshaw HM, Quist WC, Serrallach E, Valeri CR, LoGerfo FW. Flow disturbance at the distal end-to-side anastomosis. Archives Surgery. 1980; 115(11):1280–84.
12. Bourassa MG, Enjalbert M, Campeau L, Lesperance J. Progression of atherosclerosis in coronary arteries and bypass grafts: ten years later. American Journal of Cardiology. 1984; 53(12):102C–7C.
13. Fry DL. Acute vascular endothelia changes associated with increased blood velocity gradients. Circulation Research. 1968; 22(2):165–97.
14. Caro CG, Fitz-Gerald JM, Schroter RC. Atheroma and arterial wall shear observations, correlation and proposal of a shear dependent mass transfer mechanism for atherogenesis. Proc R Soc Lond B Biol Sci. 1971 Feb 16; 177(1046):109-59.
15. Ku DN, Gidden DP, Zarins CK, Glagov S. Pulsatile flow and atherosclerosis in the human carotid bifurcation. Arteriosclerosis. 1985; 5(3):293–302.
16. Ku DN, Giddens DP. Laser doppler anemometer measurements of pulsatile flow in model carotid bifurcation. Journal of Biomechanics. 1987; 20(4):407–21.
17. Moore JE, Xu C, Glagov S, Zarins GK, Ku DN. Fluid wall shear stress measurements in a model of the human abdominal aorta: oscillatory behavior and relationship to atherosclerosis. Atherosclerosis. 1994; 110(2):225–40.
18. Moore JE, Ku DN. Pulsatile velocity measurements in a model of human abdominal aorta under resting condition. Journal of Biomechanical Engineering. 1994, 116(3):337–46.
19. He X, Ku DN. Pulsatile flow in the human left coronary artery bifurcation: average conditions. ASME Journal of Biomechanical Engineering. 1996; 118(1):74–82.
20. Lei M, Kleinstreuer C, Truskey GA. A focal stress gradient-dependent mass transfer mechanism for atherogenesis in branching arteries. Medical Engineering Physics. 1996; 18(4):326–32.
21. Ma P, Li X, Ku DN. Convective mass transfer in carotid bifurcation. Journal of Biomechanics. 1997; 30(6):565–71.
22. Kleinstreuer C, Hyun S, Buchanan Jr. JR, Longest PW, Archie Jr. JP, Truskey GA. Hemodynamic parameters and early intimal thickening in branching blood vessels. Critical Reviews in Biomedical Engineering. 2001; 29(1):1–64.
23. Giddens DP, Tang TD, Loth F. New York: Plenum Press: Jaffrin MY, Caro C, editors. Fluid mechanics of arterial bifurcations in biological flows. 1995; 51–68.
24. Huo Y, Choy JS, Svendsen M, Sinha AK, Ghassan S. Kassab. Effects of vessel compliance on flow pattern in porcine epicardial right coronary arterial tree. Journal of Biomechanics. 2009; 42(5):594–602.
25. Pijls NH, van Son JA, Kirkeeide RL, De Bruyne B, Gould KL. Experimental basis of determining maximum coronary, myocardial and collateral blood flow by pressure measurements for assessing functional stenosis severity before and after percutaneous transluminal coronary angioplasty. Circulation. 1993; 87(4):1354–67.
26. Kern MJ, Lerman A, Bech JW, De Bruyne B, Eeckhout E, Fearon WF, Higano ST, Lim MJ, Meuwissen M, Piek JJ, Pijls NH, Siebes M, Spaan JA. Physiological assessment of coronary artery disease in the cardiac catheterization laboratory: a scientific statement from the American Heart Association Committee on Diagnostic and Interventional Cardiac Catheterization. Council on Clinical Cardiology. Circulation. 2006; 114(12):1321–41.
27. Spaan JA, Piek JJ, Hoffman JI, Siebes M. Physiological basis of clinically used coronary hemodynamic indices. Circulation. 2006; 113(3):446–55.
28. Perktold K, Resch M, Florian H. Pulsatile non-Newtonian flow characteristics in a three-dimensional human carotid bifurcation model. ASME Journal of Biomechanical Engineering. 1991a; 113(4):464–75.
29. Perktold K, Resch M, Peter RO. Three dimensional numerical analysis of pulsatile flow and wall shear stress in the carotid artery bifurcation. Journal of Biomechanics. 1991b; 24(6):409–20.
30. Santamarina A, Weydahl E, Sigel JM, Moore JS. Computational analysis of flow in a curved tube model of the coronary arteries: effects of time-varying curvature. Annals of Biomedical Engineering. 1998; 26:944–54.

31. Taylor CA, Hughes TJR, Zarins CK. Finite element modeling of three-dimensional pulsatile flow in the abdominal aorta: relevance to atherosclerosis. Annals of Biomedical Engineering. 1998; 26(6):975–87.
32. Weydahl ES, Moore JE. Dynamic curvature strongly affects wall shear rates in a coronary artery bifurcation model. Journal of Biomechanics. 2001; 34(9):1189–96.
33. Stroud JS, Berger SA, Saloner D. Numerical analysis of flow through a severely stenotic carotid artery bifurcation. ASME Journal of Biomechanical Engineering. 2002; 124(1):9–20.
34. Zeng D, Ding Z, Friedman MH, Ethier CR. Effect of cardiac motion on right coronary artery hemodynamics. Annals of Biomedical Engineering. 2003; 31(4):420–9.
35. Ramaswamy SD, Vigmostad SC, Wahle A, Lia YG, Olszewski ME, Braddy KC, Brennan TMH, Rossen JD, Sonka M, Chandran KB. Fluid dynamics in a human left anterior descending coronary artery with arterial motion. Annals of Biomedical Engineering. 2004; 32(12):1628–41.
36. Sankaranarayanan M, Ghista DN, Chua LP, Tan YS, Kassab GS. Analysis of blood flow in an out-of-plane CABG model. American Journal of Physiology Heart and Circulatory Physiology. 2006; 291(1):H283–H295.
37. Jagannath R, Nanduri, Francisco A. Pino-Romainville, Ismail Celik. CFD mesh generation for biological flows: Geometry reconstruction using diagnostic images. An International Journal of Computers & Fluids. 2009; 38(5):1026-32.
38. Redaelli A, Rizzo G, Arrigoni S, Di Martino E, Origgi D, Fazio F, Montevecchi F. An assisted automated procedure for vessel geometry reconstruction and hemodynamic simulations from clinical imaging. Computerized Medical Imaging and Graphics. 2002; 26(3):143-52.
39. Napel S, Marks MP, Rupin GD, Dake MD, Mc Donnell CH, Song SM, Enzmann DR, Jeffrey RB. CT angiography with spiral CT and maximum intensity projection. Radiology. 1992; 185(2):607-10.
40. Anderson CM, Edelman RR, Turski PA. New York: Raven Press: Clinical magnetic resonance angiography. 1993.
41. Chandran KB, Vonesh MJ, Roy A, Greenfield S, Kane B, Greene R, McPherson DD. Computation of vascular flow dynamics from intravascular ultrasound images. Medical Engineering Physics. 1996; 18(4):295-304.
42. Foutrakis GN, Burgreen G, Yonas H, Sclabassi RJ. Construction of 3D arterial volume meshes from magnetic resonance angiography. Neurological Research. 1996; 18(4):354-60.
43. Milner JS, Moore JA, Rutt BK, Steinman DA. Hemodynamics of human carotid artery bifurcations: computational studies with models reconstructed from magnetic resonance imaging of normal subjects. Journal of Vascular Surgery. 1998; 28(1):143-56.
44. Lucas A, Rolland Y, Calon E, Duvauferrier R, Kerdiles Y. Quantification of carotid stenosis using 3D morphometer, CT angiography and conventional angiography. Journal of Cardiovascular Surgery. 2000; 41(1):73-80.
45. Yin W, Shanmugavelayudam SK, David A. Rubenstein. 3D numerical simulation of coronary blood flow and its effect on endothelial cell activation. Hilton Minneapolis, Minnesota, USA: 31st Annual International Conference of the IEEE EMBS; 2006 Sep 2-6.
46. Abraham JP, Sparrow EM, Lovik RD. Unsteady, three-dimensional fluid mechanic analysis of blood flow in plaque-narrowed and plaque-freed arteries. International Journal of Heat and Mass Transfer. 2008; 51(23-24):5633–41.
47. Gijsen FJH, Wentzel JJ, Thury A, Lamers B, Schuurbiers JCH, Serruys PW, van der Steen AF. A new imaging technique to study 3-D plaque and shear stress distribution in human coronary artery bifurcations in vivo. Journal of Biomechanics. 2007; 40(11):2349–57.
48. Brunette J, Mongrain R, Laurier J, Galaz R, Tardif JC. 3D flow study in a mildly stenotic coronary artery phantom using a whole volume PIV method. Medical Engineering & Physics. 2008; 30(9):1193–1200.
49. Torii Ryo, Wood NB, Hughes AD, Thom SA, Sierra JA, Davies JE, Francis DP, Parker KH, Xu XY. A computational study on the influence of catheter-delivered intravascular probes on blood flow in a coronary artery model. Journal of Biomechanics. 2007; 40(11):2501–09.
50. Perktold K, Hofer M, Rappitsch G, Loew M, Kuban BD, Friedman MH. Validated computation of physiologic flow in a realistic coronary artery branch. Journal of Biomechanics. 1998; 31:217-28.
51. Melchionna S, Bernaschi M, Succi S, Kaxiras E, Rybicki FJ, Mitsouras D, Coskun AU, Feldman CL. Hydrokinetic approach to large-scale cardiovascular blood flow. Computer Physics Communications. 2010; 181(3):462–72.
52. Kenjeres S. Numerical analysis of blood flow in realistic arteries subjected to strong non-uniform magnetic fields. International Journal of Heat and Fluid Flow. 2008; 29(3):752–64.
53. Jolanda J. Wentzel, F Gijsen FJH, Schuurbiers JCH, Krams R, Serruys PW, Feyter PJD, Slager CJ. Geometry guided data averaging enables the interpretation of shear stress related plaque development in human coronary arteries. Journal of Biomechanics. 2005; 38(7):1551–55.
54. Wellnhofer E, Goubergrits L, Kertzscher U, Affeld K. In-vivo coronary flow profiling based on biplane angiograms: influence of geometric simplifications on the three-dimensional reconstruction and wall shear stress calculations. Bio Medical Engineering Online. 2006. Doi: 10.1186/1475-925X-5-39. Available from: http://www.biomedical-engineering-online.com/content/5/1/39.

55. Soulis JV, Giannoglou GD, Parcharidis GE, Louridas GE. Flow parameters in normal left coronary artery tree Implication to atherogenesis. Computers in Biology and Medicine. 2007; 37(5):628–36.
56. Chaichana T, Sun Z, Jewkes J. Computation of hemodynamics in the left coronary artery with variable angulations. Journal of Biomechanics. 2011; 44(10):1869–78.
57. Beier S, Ormiston J, Webster M, Cater J, Gracia PM, Young A, Cowan BR. Coronary artery bifurcation haemodynamics-comparison between phase contrast MRI and computational fluid dynamics. Journal of Cardiovascular Magnetic Resonance. 2014; 16(Suppl1):P224.
58. Chua LP, Zhang J, Zhou T. Numerical study of a complete anastomosis model for the coronary artery bypass. International Communications in Heat and Mass Transfer. 2005; 32(3-4):473-82.
59. Chua LP, Tong JH, Zhou T. Numerical simulation of steady flows in designed sleeve models at distal anastomoses. International Communications in Heat and Mass Transfer. 2005; 32(5):707-14.
60. Xiong FL, Chong CK. A parametric numerical investigation on haemodynamics in distal coronary anastomoses. Medical Engineering & Physics. 2008; 30(3):311–20.
61. Shim EB, Kamm RD. Finite element analysis of blood flow via a shunt from the left ventricle to the distal segment of a stenosed coronary artey. Computers in Cardiology. 2001; 28(Cat.No.0ICH37287):377-80. Doi: 10.1109/CIC.2001.977671.
62. Bertolotti C, Deplano V. Three-dimensional numerical simulations of flow through a stenosed coronary bypass. Journal of Biomechanics. 2000; 33(8):1011–22.
63. Kakos GS, Oldham HN, Dixon SH, Davis RW, Hagen PO, Sabiston Jr. DC. Coronary artery hemodynamics after aorto-coronary artery vein bypass. Journal of Thoracic and Cardiovascular Surgery. 1972; 63(6):849-53.
64. Politis AK, Stavropoulos GP, Christolis MN, Panagopoulos PG, Vlachos NS, Markatos NC. Numerical modelling of simulated blood flow in idealized composite arterial coronary grafts: Transient flow. Journal of Biomechanics. 2008; 41(1):25–39.
65. Fei DY, Thomas JD, Rittgers SE. The effect of angle and flow rate upon hemodynamics in distal graft anastomoses: a numerical model study. ASME Journal of Biomechanical Engineering. 1994; 116(3):331–6.
66. Inzoli F, Migliavacca F, Pennati G. Numerical analysis of steady flow in aorto-coronary bypass 3-D model. ASME Journal of Biomechanical Engineering. 1996; 118(2):172–9.
67. Bertolotti C, Deplano V, Fuseri J, Dupouy P. Numerical and Experimental Models of Post-Operative Realistic Flows in Stenosed Coronary Bypasses. Journal of Biomechanics. 2001; 34(8):1049–64.
68. Freshwater IJ, Morsi YS, Lai T. The effect of angle on wall shear stresses in a LIMA to LAD anastomosis: numerical modelling of pulsatile flow. Proceedings of the Institution of Mechanical Engineers. Part H: Journal of Engineering in Medicine. 2006; 220(7):743–57.
69. Kim YH, Chandran KB, Bower TJ, Corson JD. Flow dynamics across end-to-end vascular bypass graft anastomoses. Annals of Biomedical Engineering. 1993; 21(4):311–20.
70. Kute SM, Vorp DA. The effect of proximal artery flow on the hemodynamics at the distal anastomosis of a vascular bypass graft: computational study. Journal of Biomechanical Engineering. 2001; 123(3):277–83.
71. Bonert M, Myers JG, Fremes SE, Ethier CR. Orlando, FL: Influence of graft/host diameter ratio on the hemodynamics in sequential ita anastomoses. American Society of Mechanical Engineers. Bioengineering Division (Publication) BED: Advances in Bioengineering. 2000; 48:265–66.
72. Bonert M, Myers JG, Fremes S, Williams J, Ethier CR. A numerical study of blood flow in coronary artery bypass graft side-to-side anastomoses. Annals of Biomedical Engineering. 2002; 30(5):599–611.
73. Qiao A, Liu Y. Influence of graft–host diameter ratio on the hemodynamics of CABG. Bio-Medical Materials and Engineering. 2006; 16(3):189–201.
74. Owida AA, Do H, Morsi YS. Numerical analysis of coronary artery bypass grafts: An over view. Computer Methods and Programs in Biomedicine. 2012; 108(2):689-705.
75. Benard N, Perrault R, Coisne D. Blood flow in stented coronary artery: numerical fluid dynamics analysis. San Francisco, CA, USA: 26th Annual International Conference of the IEEE EMBS; 2004 Sep 1-5.
76. Garcia J, Crespo A, Goicolea J, Sanmartin M, Garcia C. Study of the evolution of the shear stress on the restenosis after coronary angioplasty. Journal of Biomechanics. 2006; 39:799–805.
77. Hsiao HM, Lee KH, Liao YC, Cheng YC. Hemodynamic Simulation of Intra-stent Blood Flow. IUMRS-ICA 2011, Procedia Engineering. 2012b; 36:128-36. Doi: 10.1016/j.proeng.2012.03.020.
78. John F LaDisa, Lars E Olson, Hettrick A Douglas, David C Warltier, Judy R Kersten, Paul S Pagel. 2006, Alterations in regional vascular geometry produced by theoretical stent implantation influence distributions of wall shear stress: analysis of a curved coronary artery using 3D computational fluid dynamics modelling**.** BioMedical Engineering Online. 2006. Doi: 10.1186/1475-925X-5-40. Available from: http://www.biomedical-engineering-online.com/content/5/1/40.
79. Chiastra C, Morlacchi S, Pereira S, Dubini G, Migliavacca F. Computational fluid dynamics of stented coronary bifurcations studied with a hybrid discretization method. European Journal of Mechanics B/Fluids. 2012; 35:76-84. Doi: 10.1016/j.euromechflu.2012.01.011.

80. Dehlaghi V, Shadpoor MT, Najarian S. Analysis of wall shear stress in stented coronary artery using 3D computational fluid dynamics modelling. Journal of materials processing technology. 2008; 197:174–181.
81. Hsiao HM, Lee KH, Liao YC, Cheng YC. Cardiovascular stent design and wall shear stress distribution in coronary stented arteries. Micro & Nano Letters. The Institution of Engineering and Technology. 2012a; 7(5):430–33.
82. Murphy J, Boyle F. Assessment of the Effects of Increasing Levels of Physiological Realism in the Computational Fluid Dynamics Analyses of Implanted Coronary Stents. Vancouver, British Columbia, Canada: 30th Annual International IEEE EMBS Conference. 2008 Aug 20-24.
83. Balossino Rossella, Gervaso Francesca, F Migliavacca F, Dubini G. Effects of different stent designs on local hemodynamics in stented arteries. Journal of Biomechanics. 2008; 41(5):1053-61.
84. Morris PD, Desmond Ryan D, Morton AC, Lycett R, Lawford PV, Hose DR, Gunn JP. Virtual Fractional Flow Reserve from Coronary Angiography: Modeling the Significance of Coronary Lesions. JACC: CARDIOVASCULAR INTERVENTIONS. 2013; 6(2):149-157.
85. Gao F, Li G, Hu R, Okada H. Computational Fluid Dynamic Analysis of Coronary Artery Stenting. International Journal of Bioscience, Biochemistry and Bioinformatics. 2014; 4(3):155-59.
86. Chen J, Lu XY, Wang W. Non-Newtonian effects of blood flow on hemodynamics in distal vascular graft anastomoses. Journal of Biomechanics. 2006; 39(11):1983–95.
87. Do H, Owida AA, Yang W, Morsi YS. Numerical simulation of the haemodynamics in end-to-side anastomoses. International Journal for Numerical Methods in Fluids. 2010 Sep 7. Doi: 10.1002/fld.2381.
88. Lee D, Su JM, Liang HY. A numerical simulation of steady flow fields in a bypass tube. Journal of Biomechanics. 2001; 34(11):1407–16.
89. Politis AK, Stavropoulos GP, Christolis MN, Panagopoulos FG, Vlachos NS, Markatos NC. Numerical modeling of simulated blood flow in idealized composite arterial coronary grafts: steady state simulations. Journal of Biomechanics. 2007; 40(5):1125–36.
90. Vimmr J, Jonasova A. Non-Newtonian effects of blood flow in complete coronary and femoral bypasses. Mathematics and Computers in Simulation. 2010; 80(6):1324–36.
91. Zhang JM, Chua LP, Ghista DN, Zhou TM, Tan YS. Validation of numerical simulation with PIV measurements for two anastomosis models. Medical Engineering and Physics. 2008; 30(2):226–47.